IEEE Photonics Journal
An IEEE Photonics Society Publication

Open Access

Microdisk Resonator With Negative Thermal Optical Coefficient Polymer for Refractive Index Sensing With Thermal Stability

Volume 10, Number 2, April 2018

Tao Ma
Jinhui Yuan
Feng Li
Lei Sun
Zhe Kang
Binbin Yan
Qiang Wu
Xinzhu Sang
Kuiru Wang
Heng Liu
Fang Wang
Bo Wu
Chongxiu Yu
Gerald Farrell

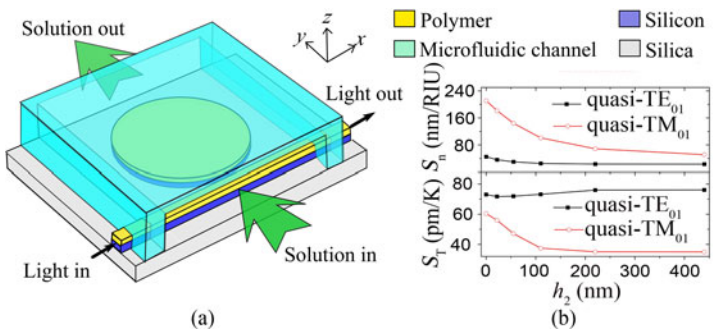

DOI: 10.1109/JPHOT.2018.2811758
1943-0655 © 2018 IEEE

Microdisk Resonator With Negative Thermal Optical Coefficient Polymer for Refractive Index Sensing With Thermal Stability

Tao Ma [1,2] Jinhui Yuan [2,3] Feng Li [3] Lei Sun [2] Zhe Kang,[3] Binbin Yan,[2] Qiang Wu [4] Xinzhu Sang,[2] Kuiru Wang,[2] Heng Liu,[1] Fang Wang,[1] Bo Wu [1] Chongxiu Yu,[2] and Gerald Farrell[5]

[1]College of Electronic and Electrical Engineering, Henan Normal University, Xinxiang 453007, China
[2]State Key Laboratory of Information Photonics and Optical Communications, Beijing University of Posts and Telecommunications (BUPT), Beijing 100876, China
[3]Photonics Research Centre, Department of Electronic and Information Engineering, The Hong Kong Polytechnic University, Hung Hom, Hong Kong
[4]Department of Physics and Electrical Engineering, Northumbria University, Newcastle Upon Tyne, NE1 8ST, U.K.
[5]Photonics Research Center, School of Electronic and Communications Engineering, Dublin Institute of Technology, Dublin 8 D08 X622, Ireland

DOI:10.1109/JPHOT.2018.2811758

Manuscript received January 21, 2018; revised February 20, 2018; accepted February 28, 2018. Date of publication March 13, 2018; date of current version March 27, 2018. This work was supported in part by the Government of Ireland Scholarship in the College of Engineering and Built Environment, in part by the National Natural Science Foundation of China under Grant 61475023, in part by the Beijing Youth Top-Notch Talent Support Program under Grant 2015000026833ZK08, in part by the Natural Science Foundation of Beijing under Grant 4152037, in part by the Fund of State Key Laboratory of Information Photonics and Optical Communications P. R. China under Grants IPOC2016ZT05 and IPOC2017ZZ05, in part by the Key Project of Henan Education Department under Grant 15A510029, and in part by the Young Foundation of Henan Normal University under Grant 2015QK05, and in part by the scientific and technological project of Henan province (182102310712 and 182102210367) which are hosted by Tao Ma and Fang Wang, respectively. Corresponding authors: Jinhui Yuan and Feng Li (e-mail: yuanjinhui81@163.com; enlf@polyu.edu.hk).

Abstract: In this paper, we propose a microdisk resonator with negative thermal optical coefficient (TOC) polymer for refractive index (RI) sensing with thermal stability. The transmission characteristics and sensing performances by using quasi-TE_{01} and quasi-TM_{01} modes are simulated by a three-dimensional finite element method. The influences of the TOC, RI, and thickness of the polymer on the sensing performances are also investigated. The simulation results show that the RI sensitivity S_n and temperature sensitivity S_T with different polymers are in the ranges of 25.1–26 nm/RIU and 67.3–75.2 pm/K for the quasi-TE_{01} mode, and 94.5–110.6 nm/RIU and 1.2–51.3 pm/K for the quasi-TM_{01} mode, respectively. Moreover, figure-of-merit of the temperature sensing for the quasi-TM_{01} mode is in the range of 2×10^{-4}–8×10^{-3}, which can find important application in the implementation of the adiabatic devices.

Index Terms: Microdisk resonator, sensors, refractive index, temperature.

1. Introduction

Silicon based photonic integrated circuit (PIC) platform has attracted much interest in past decades [1]. Particularly, silicon photonic configurations were widely adopted as optical sensors in environmental and biomedical applications. Silicon is suitable for many spectroscopic sensing applications benefiting from its wide transparent spectral window, which covers from 1100 nm to 6500 nm. The rapid development of complementary metal-oxide semiconductor (CMOS) technique has greatly promotes the evolution of the PIC technology [2], [3]. Up to now, silicon-on-insulator (SOI) platform is mostly adopted in the design and fabrication of PICs due to the CMOS compatibility. Moreover, SOI waveguide has a large refractive index (RI) contrast between the silicon core and the silica substrate, which can reduce the cross section of waveguide to nanometer scale.

In the course of miniaturization of photonic devices, high quality factor (Q factor) micro-resonators, including micro-rings, racetracks, toroids, microdisks, and spheres, have attracted much attention due to their remarkable enhancements of light-matter interaction and wide applications in sensing, metrology and nonlinear optics [4]–[9]. Among these micro-resonators, microdisk resonators as whispering gallery resonators are CMOS compatible and can be easily fabricated. Compared with micro-ring resonators, microdisk resonators can achieve small footprint, wide free spectral ranges (FSRs), and high Q factors [10], [11]. These advantages are beneficial to improve the sensing performances for sensing applications [12], [13]. However, the SOI microdisks show vulnerability to the temperature change due to high thermo-optic coefficient of the silicon material (1.86×10^{-4} K^{-1}) and wavelength selectivity of the microdisks [14]. To reduce or eliminate the temperature effect, reference configurations [15], temperature control devices [16], and negative thermal optical coefficient (TOC) polymer [17] cladding are proposed. Compared with reference configurations and temperature control devices, temperature compensation by negative TOC polymers, which are also used to fabricate microfluidic channels in biological and chemical sensing, has advantages including convenient preparation, power saving, and easy integration. Furthermore, the polymer layers can also be used as the effective enrichment layers for specific analytes to functionalize the microdisk resonator based sensor devices [18].

In this paper, we propose an SOI based microdisk resonator with a negative TOC polymer cover layer for RI sensing with thermal stability. The propagating modes and transmission response of the microdisk resonator are characterized by three-dimensional finite element method (3D-FEM). The effective RI (n_{eff}) and waveguide sensitivity (S_{wg}) of both quasi-TE$_{01}$ and quasi-TM$_{01}$ modes are investigated. The transmission spectra and coupling properties with different coupling gaps (W_{gap}) are also demonstrated. Subsequently, the RI sensing performances including sensitivity and figure-of-merit (FOM) are analyzed. The microdisk resonator proposed can be easily fabricated with standard CMOS technique.

2. Microdisk Resonator Design

The schematic of the proposed SOI microdisk resonator with a polymer cladding is shown in Fig. 1(a). A layer of negative TOC polymer (polymethyl methacrylate, PMMA, RI of 1.49) is deposited on the silicon layer (RI$\sim$3.5) of an SOI wafer before the fabrication of the waveguide. The polymer and silicon layers are etched with a same pattern thus the silicon waveguide is sandwiched between the top polymer cladding and the bottom silica substrate (RI$\sim$1.45). The cross-section of the waveguide (y-z plane) is shown in Fig. 1(b), where the geometrical dimensions are labeled. The diameter (D) of the microdisk resonator is 4 μm. The width of the bus waveguide is w. The thicknesses of the silicon and polymer layers are h_1 and h_2 respectively. The gap separation between the bus waveguide and the microdisk is W_{gap}. W_{gap}, w, h_1, and h_2 will be optimized in the following simulations. The probe optical signal can be coupled in/out the waveguide from/to an optical fiber via an in-plane grating coupler [19]. In order to investigate the sensing performance, a prefabricated U shaped microfluidic channel is inversely placed to cover the microdisk resonator. Thus the whole resonator and the coupling section of the bus waveguide will be immersed in the flowing solutions with RI n_{c} injected into the microfluidic channel [20].

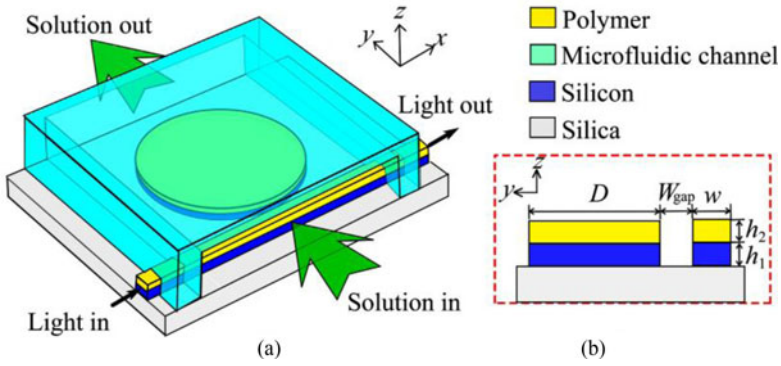

Fig. 1. (a) Schematic architecture of the double-layers microdisk resonator and (b) the cross-section of the *y*–z plane of the waveguide.

The propagating modes and transmission response of the microdisk resonator will be investigated by 3D-FEM, which is widely used in the characterization of integrated photonic devices [21], [22].

3. Characterization of the Microdisk Resonator

3.1 Modes Characteristics

During the propagation in the long bus waveguide between the input grating and the coupling point to the microdisk resonator, the light other than the propagation modes supported by the bus waveguide will leak out. We consider the propagation modes of the bus waveguide only as the input field, which are obtained by boundary mode analysis with scattering boundary condition in simulation. The wavelength of the input light is fixed at 1550 nm. The upper cladding of the microdisk is aqueous solution (RI~1.33).

The mode field distributions and corresponding effective refractive indices with different w and h_2 are shown in Fig. 2(a) and (b), respectively. The propagation modes are classified into two groups as quasi-TE or quasi-TM modes. Since the confinement of mode field in the silicon layer of quasi-TE modes is better than that of quasi-TM modes, the quasi-TE modes have much larger n_{eff} than quasi-TM modes. With a given h_2, the number of modes increases as w increases. The influences of h_2 on n_{eff} for quasi-TM modes are much greater than that for quasi-TE modes because of the larger penetration depth into the polymer layer of quasi-TM modes. When w is chosen as 500 nm, only quasi-TE_{01} and quasi-TM_{01} modes exist in the bus waveguide. We consider them as the injected modes in the following simulations.

Besides h_2, the thickness of silicon layer h_1 is also simulated. With h_2 values of 110 and 220 nm, the n_{eff} curves of the propagation modes with different h_1 are shown in Fig. 3(a) and (b), respectively. With the increase of h_1, the portion of mode field that confined in the silicon layer will increase, which will increase the n_{eff} and simultaneously the number of modes. If the mode field is well confined in the silicon layer, obviously the impact of the polymer layer will be weakened. It can be observed from Fig. 3 that the differences between the n_{eff} curves with $h_2 = 110$ and 220 nm are gradually reduced along the increase of h_1.

The sensitivity (S) is a crucial parameter for evaluating the sensing performance. Here, the RI sensitivity (S_{n}) and temperature sensitivity (S_{T}) are respectively defined as the resonant wavelength shift ($\Delta\lambda_{\text{res}}$) versus the solution RI change (Δn_{c}) and the temperature change (ΔT) of the analytes as follows

$$S_{\text{n}} = \frac{\Delta\lambda}{\Delta n_c} = \frac{\Delta\lambda}{\Delta n_{\text{eff}}} \cdot \frac{\Delta n_{\text{eff}}}{\Delta n_c} = S_{\text{dev}} S_{\text{wg,n}},$$
$$S_{\text{T}} = \frac{\Delta\lambda}{\Delta T} = \frac{\Delta\lambda}{\Delta n_{\text{eff}}} \cdot \frac{\Delta n_{\text{eff}}}{\Delta T} = S_{\text{dev}} S_{\text{wg,T}}, \quad (1)$$

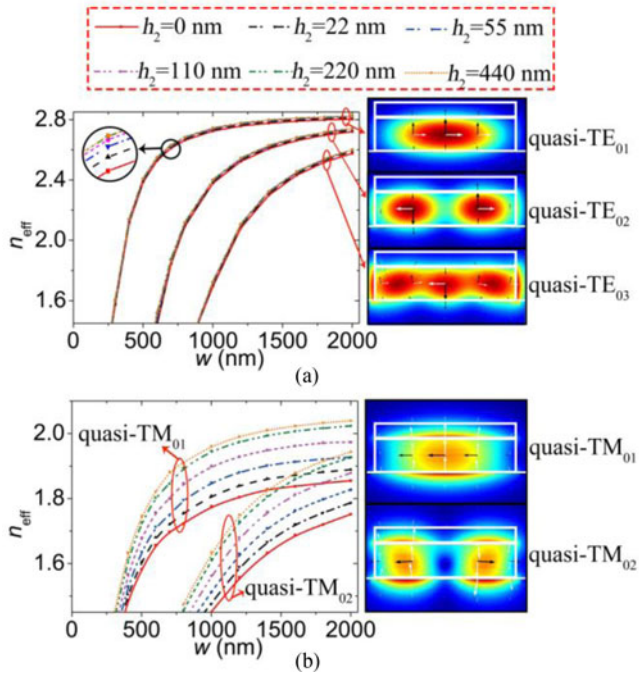

Fig. 2. Effective refractive indices of (a) quasi-TE mode and (b) quasi-TM mode of the bus waveguide as a function of w with different h_2 and a fixed h_1 of 220 nm at the wavelength of 1550 nm. The insets show the corresponding mode field distributions of the quasi-TE mode and quasi-TM mode calculated at 1550 nm, respectively, the white and black arrows indicating the electric and magnetic field directions.

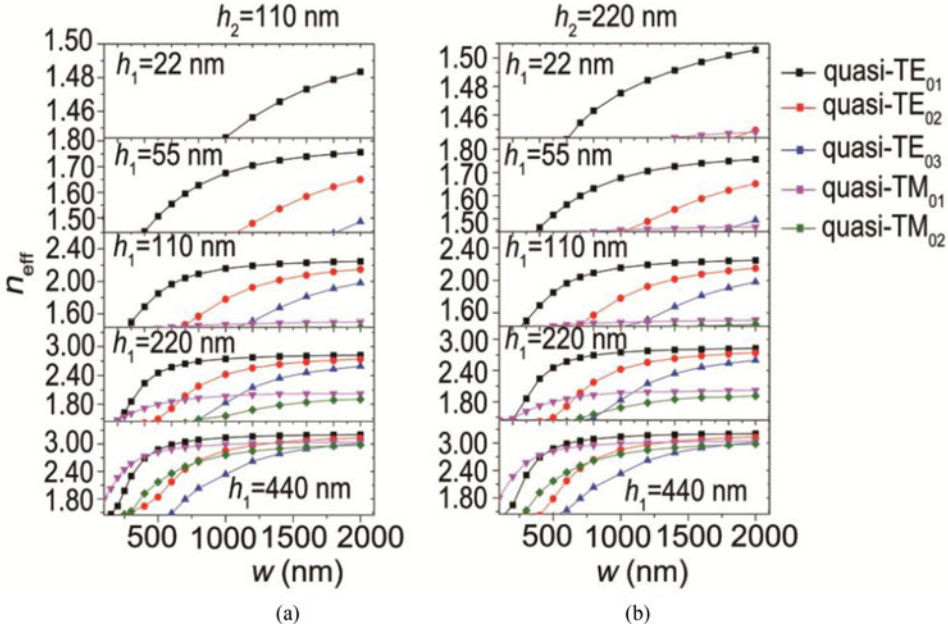

Fig. 3. Effective refractive indices of the modes propagate in the bus waveguide as a function of w with different h_1 and a fixed h_2 of (a) 110 nm and (b) 220 nm at the wavelength of 1550 nm.

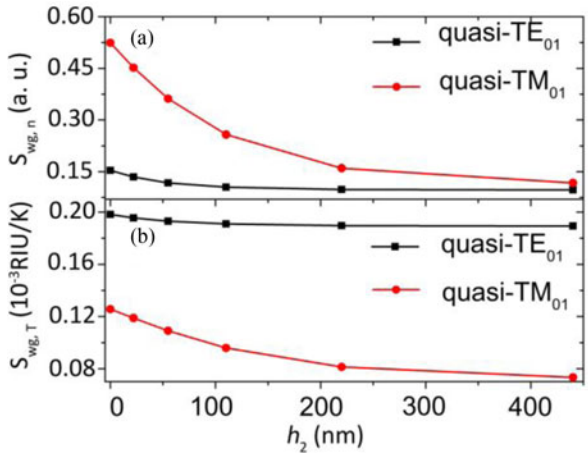

Fig. 4. Influences of h_2 on (a) $\Delta S_{wg,n}$ and (b) $\Delta S_{wg,T}$ for quasi-TE_{01} and quasi-TM_{01} modes.

where Δn_{eff} is the change of n_{eff} and $S_{dev} = \Delta\lambda/\Delta n_{eff}$ is the device sensitivity. $S_{wg,n} = \Delta n_{eff}/\Delta n_c$ and $S_{wg,T} = \Delta n_{eff}/\Delta T$ are the waveguide sensitivities of the RI and temperature sensing, which depend on the waveguide structures.

In order to enhance the overall sensitivity, it is necessary to optimize both the device and waveguide sensitivities. Here, the variations of $S_{wg,n}$ and $S_{wg,T}$ versus h_2 for quasi-TE_{01} and quasi-TM_{01} modes are shown in Fig. 4(a) and (b), respectively. From Fig. 4(a) and (b), both $S_{wg,n}$ and $S_{wg,T}$ reduce with the increase of h_2 where the sensitivity variation of quasi-TE_{01} mode is more significant than that of quasi-TM_{01} mode. While comparing the sensitivities of the two modes, the sensor has a much higher RI sensitivity $S_{wg,n}$ but a lower temperature sensitivity $S_{wg,T}$ for quasi-TM_{01} mode than that of quasi-TE_{01} mode.

3.2 Transmission Responses

Besides the sensitivity, the Q factor of the microdisk will determine the spectral resolution and affect other performance of the sensor in the measurement of spectral shift [23]. Q factor can be calculated by

$$Q = \lambda/\delta, \tag{2}$$

where λ_{res} is the central wavelength and δ is the full width at half maximum of the resonant peak used for sensing. Another important parameter for evaluating the sensing performance of the microdisk resonator is the extinction ratio (ER), which is defined as

$$ER = -10\log_{10}(H_{max}/H_{min}), \tag{3}$$

where H_{max} and H_{min} are respectively the maximum and minimum on the transmission spectrum of the device.

The transmission spectra with different W_{gap} for the quasi-TE_{01} and quasi-TM_{01} modes are simulated. The Q factor and ER of the resonance peaks near wavelength 1550 nm are obtained from the transmission spectra, as shown in Fig. 5(a) and (b), respectively. The different curves are obtained with different h_2 varying from 0 to 440 nm. The Q factor increases monotonically with the increase of W_{gap} from 0 to 200 nm. However, the ER first increases to the maximum value with a critical coupling, and then decreases sharply. With the increase of h_2 from 22 to 440 nm, W_{gap} of the critical coupling increases from 43 to 60 nm. Therefore, there is a trade-off between the Q factor and ER. A larger W_{gap} will result in a higher Q factor but a smaller ER. When a value of 80 nm is chosen for W_{gap}, the corresponding ER varies from 9 to 14.5 dB when h_2 varies from 22 to 440 nm. For the quasi-TM_{01} mode, critical coupling can also be obtained when W_{gap} is $\sim$30 nm. The Q factor of quasi-TM_{01} mode is much lower than that of quasi-TE_{01} mode. The variations of the Q factor and ER curves are similar to that of the quasi-TE_{01} mode except for the curves with near zero h_2.

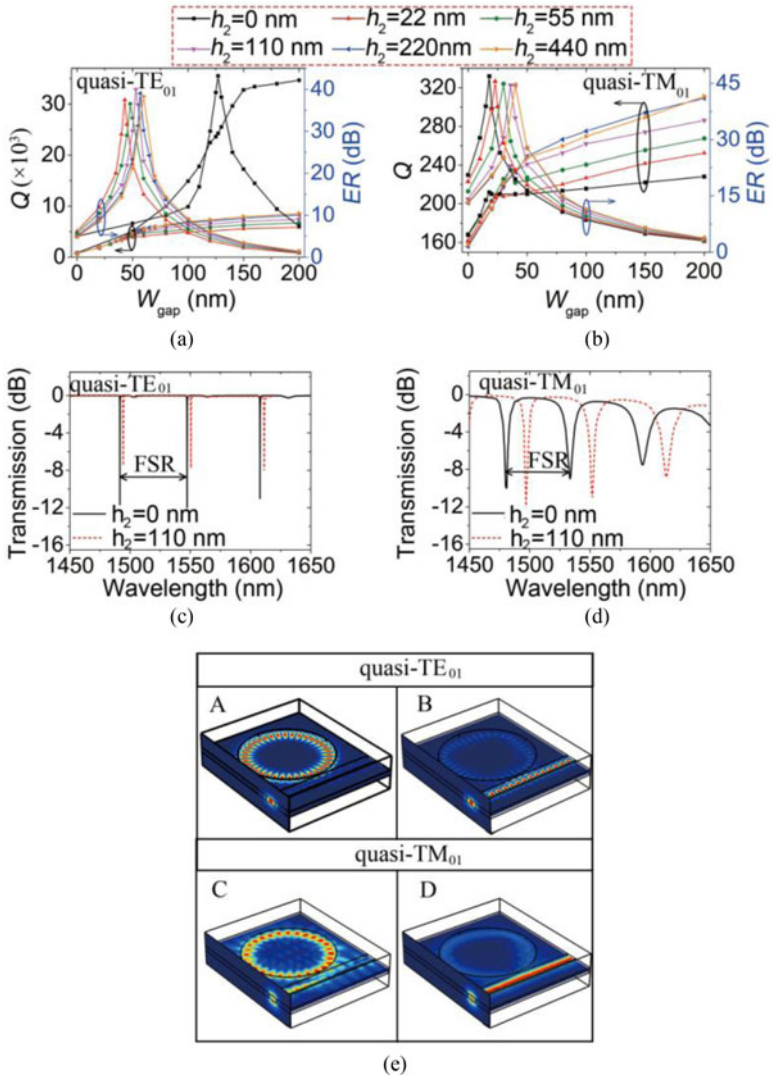

Fig. 5. The variations of Q factor and ER versus W_{gap} with different h_2 for (a) quasi-TE_{01} mode and (b) quasi-TM_{01} mode. The transmission spectra of (c) quasi-TE_{01} mode and (d) quasi-TM_{01} mode with h_2 of 0 and 110 nm. (e) The optical field distributions with a 1550 nm CW pump for quasi-TE_{01} mode (A, B) and quasi-TM_{01} mode (C, D) in microdisk resonators with (A, C) and without (B, D) the 110 nm polymer layer.

From Fig. 5(a), the quasi-TE_{01} mode is very sensitive to the polymer layer. The introduction of a very thin polymer layer with $h_2 = 22$ nm leads to great changes of the curves for quasi-TE_{01} mode. But the changes of the curves for quasi-TM_{01} mode are very minor with such thin polymer layer. Due to the different polarized directions of the quasi-TE_{01} mode and the quasi-TM_{01} mode, their coupling strengths between the bus waveguide and microdisk resonator have different changes after introducing the polymer layer. Then the coupling strength induces the significantly different variations of the Q factor and ER curves in Fig. 5(a) and (b).

When W_{gap} is chosen as 80 nm, the transmission spectra of the microdisk resonator for the quasi-TE_{01} and quasi-TM_{01} modes are shown in Fig. 5(c) and (d), respectively. The free spectral range (FSR) of the transmission spectra is ~60 nm for both modes. The black solid ($h_2 = 0$ nm) and red dashed ($h_2 = 110$ nm) curves represent the transmission spectra with and without the upper polymer layer, respectively. When the upper polymer layer is introduced, the ER of the transmission spectrum decreases for quasi-TE_{01} mode but increases for quasi-TM_{01} mode. It should be noted that

the wavelength 1550 nm is the resonant wavelength of both quasi-TE_{01} and quasi-TM_{01} modes with the 110 nm polymer layer. Without the polymer layer, the wavelength 1550 nm will be off-resonant for both modes.

The optical field distributions in microdisk resonators with and without the 110 nm polymer layer, which are pumped with a 1550 nm CW light, are shown in Fig. 5(e). For the quasi-TE_{01} mode, the on-resonant state with the polymer layer and the off-resonant state without the polymer layer are shown in the insets A and B, respectively. The field distributions for the quasi-TM_{01} mode are shown in C and D accordingly. From Fig. 5(e), high intensity optical fields in the microdisk resonator are established with an on-resonant pump but the intra cavity fields are very weak with an off-resonant pump.

4. Sensing Performances and Proposed Fabrication Process

4.1 RI Sensing and Thermal Stability

In applications, the solutions flowing in the microfluidic channel will have different RIs with different concentrations. For aqueous solutions, the RI n_c will be a little higher than the RI of water. We characterize the transmission spectra of the microdisk resonator with h_2 of 110 nm and a varying n_c from 1.33 to 1.39. The transmission spectra with the quasi-TE_{01} and quasi-TM_{01} modes are shown in Fig. 6(a) and (b), respectively. The resonant wavelengths are shifted towards long wavelength by 1.42 nm for quasi-TE_{01} mode and 6.38 nm for quasi-TM_{01} mode with the increase of n_c for both modes. With increasing of n_c, the *ER* of quasi-TE_{01} mode increases along the shift but a decrease of *ER* is observed for quasi-TM_{01} mode. When the cladding RI (n_c) increases, the field confinement in core of waveguide weaken. On the other hand, the electric fields in cladding of waveguide enhance. As a results of the different polarized directions of the quasi-TE_{01} mode and the quasi-TM_{01} mode, their enhancement of electric fields in cladding are on different directions. For the quasi-TE_{01}, the electric field increases in the horizontal direction (*y* axis). It is benefit for the coupling between the bus waveguide and microdisk resonator. The couple state remains closer to the critical coupling from under coupling, hence the *ER* of the transmission increases as shown in Fig. 6(a). However, for the quasi-TM_{01}, the couple state has the opposite effect due to its electric field increases on the vertical direction (*z* axis). Therefore, the *ER* of the transmission decrease as shown in Fig. 6(b).

The temperature sensitivity S_T is used to evaluate the thermal stability. To analyze S_T, we include the TOCs of the materials to calculate the RI changes of the waveguide caused by the temperature variation. At the temperature of 295 K and wavelength of 1550 nm, the TOCs of Si, SiO_2, PMMA and water are about 1.8×10^{-4}/K, 2.8×10^{-5}/K, -1.1×10^{-4}/K and -9.9×10^{-5}/K, respectively [24]. The thermal shifts of the resonances for quasi-TE_{01} and quasi-TM_{01} modes are investigated with a temperature variation of $\pm$20 K, as shown in Fig. 6(c) and (d). When the relative temperature ΔT varies from $-$20 K to 20 K, the resonant wavelength increases by 2.92 nm for quasi-TE_{01} mode and 1.54 nm for quasi-TM_{01} mode, respectively.

The sensitivities S_n and S_T with different h_2 are shown in Fig. 6(e). Compare with Figs. 4 and 6(e), the changes of waveguide sensitivity ($S_{wg,n}$ and $S_{wg,n}$) are similar with the total sensitivity (S_n and S_T). As shown in Figs. 4 and 6(e), with the increase of h_2, S_n and S_T for quasi-TM_{01} mode decrease sharply when h_2 is less than 110 nm, and then the variations become very slow. For quasi-TE_{01} mode, the variations of S_n and S_T are much lower than that of quasi-TM_{01} mode. To understand the difference of the two modes, the vertical intensity distributions in the waveguide along the z direction are shown in Fig. 6(f) with different h_2. The dashed vertical lines indicate the positions of the top surface of the polymer layer with different thickness.

For quasi-TE_{01} mode, the field intensity in the polymer layer is much lower than that in the Si layer. In contrast, the field intensity of quasi-TM_{01} mode is much stronger in the polymer layer and upper cladding (solutions) than that in the Si layer. Thus, the RI sensitivity S_n for quasi-TE_{01} mode is smaller than that for quasi-TM_{01} mode because of the lower intensity in the upper cladding. On another side, high intensity in the negative TOC polymer layer of the quasi-TM_{01} mode has naturally reduced its temperature sensitivity S_T comparing with that of quasi-TE_{01} mode. With the increase

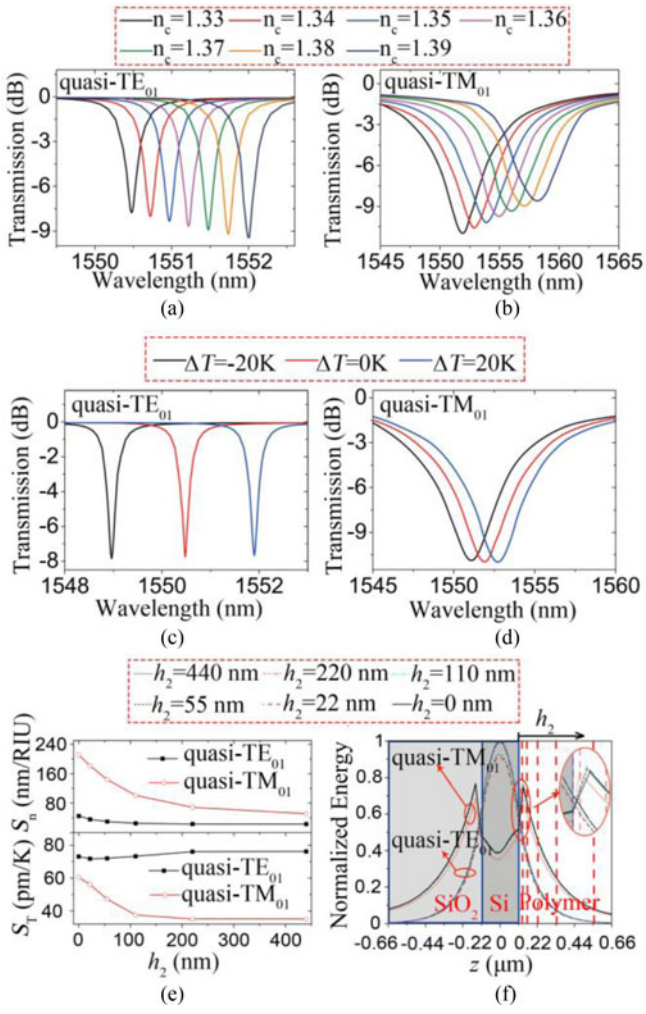

Fig. 6. Transmission spectra with different n_c for (a) quasi-TE_{01} mode and (b) quasi-TM_{01} mode. Transmission spectra with different T for (c) quasi-TE_{01} mode and (d) quasi-TM_{01} mode.(e) S_n and S_T with different h_2, and (f) field energy of the waveguide along z axis with different h_2.

of h_2, the interaction between the optical field of quasi-TM_{01} mode and the surrounding solutions are significantly affected especially when the top surface of the polymer layer is close to the peak position of the field intensity. Hence the sensitivities S_n and S_T are both reduced quickly in this region. When the top surface of the polymer layer is far from the peak of the field intensity, the impact of the polymer layer thickness becomes very weak. For quasi-TE_{01} mode, the variations of S_n and S_T caused by the increase of h_2 are much smaller than that of quasi-TM_{01} mode.

To be more realistic, we investigate the sensing performance with adoption of several different polymers including CYTOP, PDMS, PMMA, DR1/PMMA, and SU-8 as a 110 nm coating layer. The RI (n_p) and TOCs (t_p) of these polymers are listed in Table 1. For comparison, the difference of sensitivities between these polymers and the CYTOP is shown in Fig. 7. ΔS_n and ΔS_T represent the relative changes of S_n and S_T comparing with the CYTOP layer covered resonator. S_n for quasi-TE_{01} and quasi-TM_{01} modes with the CYTOP layer are 94.5nm/RIU and 25.1nm/RIU, respectively. The relative change ΔS_n with different polymers are shown in Fig. 7(a) at different n_p for the different polymers. With the increase of n_p, ΔS_n increases by 16 nm/RIU for quasi-TM_{01} mode but only 0.8 nm/RIU for quasi-TE_{01} mode. S_T for quasi-TE_{01} and quasi-TM_{01} modes are 75.2 pm/K and 51.3 pm/K respectively with CYTOP layer. The influence on ΔS_T by different t_p of different polymers

TABLE 1
RI and TOCs of Several Polymers

Polymers	RI	TOC ($\times 10^{-4}$ K^{-1})	Ref.
CYTOP	1.34	−0.5	[25]
PDMS	1.41	−4.66	[26]
PMMA	1.49	−1.1	[27]
DR1/PMMA	1.49∼1.51	−1.1∼−1.35	[28]
SU-8	1.58	−1.8	[29]

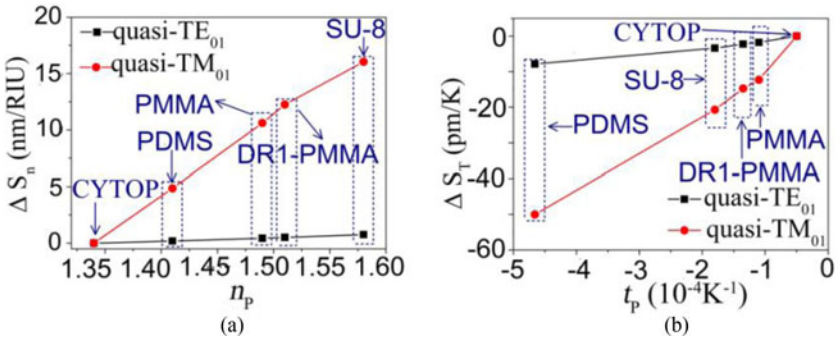

Fig. 7. Changes of (a) ΔS_n and (b) ΔS_T of S_n and S_T for the polymers with different n_p and TOCs.

is shown in Fig. 7(b). ΔS_T decreases quickly for quasi-TM$_{01}$ mode with decrease of t_p. When t_P decreases to -4.66×10^{-4} K^{-1} by using PDMS polymer, ΔS_T is ~ -50 pm/K for quasi-TM$_{01}$ mode but only -8 pm/K for quasi-TE$_{01}$ mode. The influence of the TOC on ΔS_T for quasi-TM$_{01}$ mode is greater than that for quasi-TE$_{01}$ mode.

To compare the sensing performance with other sensing structures, the figure-of-merit (FOM) is used to evaluate the sensing performance [30], [37]. It is defined as the ratio between the sensitivity S and δ as following

$$\text{FOM} = S/\delta = S(Q/\lambda_{\text{res}}). \tag{4}$$

In our work, the δs of the transmission spectra for quasi-TE$_{01}$ and quasi-TM$_{01}$ modes are ∼0.25 and ∼5.9 nm, respectively. Taking into account of the negative TOC polymers, the FOMs of the S_n and S_T for quasi-TE$_{01}$ mode are in the ranges of 101∼104 and 0.25∼0.28, respectively. Meanwhile FOMs of S_n and S_T for quasi-TM$_{01}$ mode are in the ranges of 16∼19 and 2×10^{-4}∼8×10^{-3}, respectively.

The RI and temperature sensing performances for different configurations are compared in Table 2. The proposed microdisk resonator based sensor achieves the lowest S_T of 1.2 pm/K and FOM of 2×10^{-4}, which are beneficial to reduce the thermal effect of integrated devices. Moreover, the proposed CMOS compatible sensor is easy to fabricate and integrate compared with cascaded microring [31], microsphere [32], and microbubble [33].

4.2 Proposed Fabrication Process

In experiments, the microdisk resonator can be fabricated by using the standard CMOS technique [19] and nanoimprint technique [38], [39]. The nanoimprint technique is widely applied to a variety

TABLE 2
Comparison of the RI and Temperature Sensing Performances Between Different Configurations

Configuration	modes	S_n(nm/RIU)	S_T(pm/K)	δ (nm)	FOM of RI sensing	FOM of temperature sensing	Ref.
Waveguide grating	–	–	88.5	1.61	–	0.055	[30]
Cascaded ring	–	–	293.9	0.155	–	1.9	[31]
Microsphere	WGM	–	245	0.0015	–	163	[32]
Microbubble	WGM	–	200	0.00172	–	116	[33]
Racetrack	–	70	–	0.75	934	–	[34]
Slot ring	TE	–	27	1.56	–	0.18	[35]
Microring	TE_0	104	78.7		371	0.28	[36]
	TM_0	319	34.1	0.28	1139	0.12	
Microdisk	WGM(TE_{01})	25.1∼26	67.3∼75.2	0.25	101∼104	0.25∼0.28	our work
	WGM(TM_{01})	94.5∼110.6	1.2∼51.3	5.9	16∼19	$2 \times 10^{-4} \sim 8 \times 10^{-3}$	

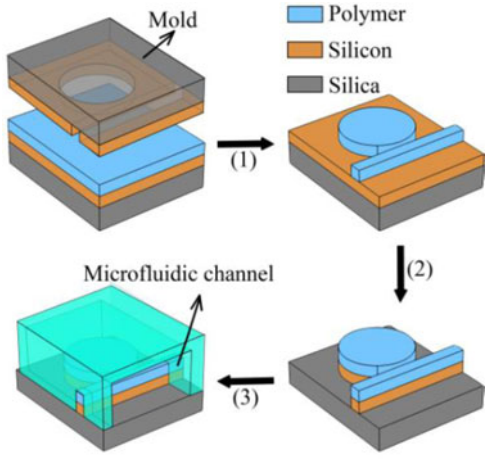

Fig. 8. Schematic diagram of the fabrication process of the proposed microdisk resonator.

of polymers due to its precise dimension control, low cost, and simple process. The pre-fabricated flexible microfluidic channel will be installed after the fabrication of the microdisk resonator [34]. The microfluidic channels can be fabricated with polyethylene (PE), polypropylene (PP), polydimethylsiloxane (PDMS), SU-8, PMMA, or SiO_2 [41]–[45]. The proposed fabrication process is illustrated in Fig. 8 as follows

1) The nanoimprint process is performed, A mold with reverse patterns of the microdisk and the bus waveguide are pressed into a thin polymer film on a silicon substrate.
2) The double-layer waveguide and microdisk are formed by the silicon etching.
3) The microfluidic channel is inversely mounted on the top of the platform.

5. Conclusion

In summary, a microdisk resonator with negative TOC polymer layer is proposed for RI sensing with thermal stability. The transmission spectra and sensing performances of the proposed microdisk resonator are characterized by the 3D-FEM. The simulation results show that the influence of the polymer upper cladding on the RIs for quasi-TM_{01} mode is greater than that for quasi-TE_{01} mode. Moreover, the investigations on Q factor and ER of the microdisk resonator indicate that the critical coupling also exists as that in the traditional microdisk resonators. The thickness of the polymer layer affects S_n and S_T greatly for quasi-TM_{01} mode but slightly for quasi-TE_{01} mode. With different negative TOC polymers, S_n of 25.1∼26 nm/RIU and S_T of 67.3∼75.2 pm/K are obtained for quasi-TE_{01}mode. For quasi-TM_{01} mode, S_n and S_T are 94.5∼110.6 nm/RIU and 1.2∼51.3 pm/K, respectively. A low temperature sensitivity of 1.2 pm/K is achieved with the proposed microdisk resonator, which is important for development of thermal stable and integrated sensing devices.

References

[1] A. Novack *et al.*, "Progress in silicon platforms for integrated optics," *Nanophotonics*, vol. 3, nos. 4–5, pp. 205–214, 2014.

[2] W. Bogaerts *et al.*, "Silicon-on-insulator spectral filters fabricated with CMOS technology," *IEEE J. Select. Topics Quantum Electron.*, vol. 16, no. 1, pp. 33–44, Jan. 2010.

[3] S. K. Selvaraja, W. Bogaerts, P. Dumon, D. Van Thourhout, and R. Baets, "Subnanometer linewidth uniformity in silicon nanophotonic waveguide devices using CMOS fabrication technology," *IEEE J. Select. Topics Quantum Electron.*, vol. 16, no. 1, pp. 316–324, Jan. 2010.

[4] A. Van Eeghem *et al.*, "Double positive effect of adding hexaethyelene glycol when optimizing the hybridization efficiency of a microring DNA detection assay," *Appl. Surf. Sci.*, vol. 405, pp. 321–328, May 2017.

[5] A. Ramachandran *et al.*, "A universal biosensing platform based on optical micro-ring resonators," *Biosens. Bioelectron.*, vol. 23, no. 7, pp. 939–944, Feb. 2008.

[6] K. J. Vahala, "Optical microcavities," *Nature*, vol. 424, pp. 839–846, Aug. 2003.

[7] R. W. Boyd and J. E. Heebner, "Sensitive disk resonator photonic biosensor," *Appl. Opt.*, vol. 40, no. 31, pp. 5742–5747, Nov. 2001.

[8] S. Yang, Y. Wang, and H. Sun, "Advances and prospects for whispering gallery mode microcavities," *Adv. Opt. Mater.*, vol. 3, no. 9, pp. 1136–1162, Aug. 2015.

[9] J. Wang, T. Zhan, G. Huang, P. K. Chu, and Y. Mei, "Optical microcavities with tubular geometry: Properties and applications," *Laser Photon. Rev.*, vol. 8, no. 4, pp. 521–547, 2014.

[10] M. Soltani, Q. Li, S. Yegnanarayanan, and A. Adibi, "Toward ultimate miniaturization of high Q silicon traveling-wave microresonators," *Opt. Exp.*, vol. 18, no. 19, pp. 19541–19557, Sep. 2010.

[11] B. Momeni *et al.*, "Silicon nanophotonic devices for integrated sensing," *J. Nanophoton.*, vol. 3, no. 1, Apr. 2009, Art. no. 031001.

[12] S. C. Eom and J. H. Shin, "Design and optimization of horizontal slot microdisk sensors," *IEEE Photon. Technol. Lett.*, vol. 25, no. 19, pp. 1859–1862, Oct. 2013.

[13] I. S. Grudinin and N. Yu, "Finite-element modeling of coupled optical microdisk resonators for displacement sensing," *J. Opt. Soc. Amer. B*, vol. 29, no. 11, pp. 3010–3014, Nov. 2012.

[14] K. Padmaraju and K. Bergman, "Resolving the thermal challenges for siliconmicroring resonator devices," *Nanophotonics*, vol. 3, nos. 4–5, pp. 269–281, Aug. 2014.

[15] H. S. Lee, G. D. Kim, and S. S. Lee, "Temperature compensated refractometric biosensor exploiting ring resonators," *IEEE Photon. Technol. Lett.*, vol. 21, no. 16, pp. 1136–1138, Aug. 2009.

[16] Q. Fang *et al.*, "High efficiency ring-resonator filter with NiSi Heater," *IEEE Photon. Technol. Lett.*, vol. 24, no. 5, pp. 350–352, Mar. 2012.

[17] J. Teng *et al.*, "Athermal silicon-on-insulator ring resonators byoverlaying a polymer cladding on narrowedwaveguides," *Opt. Exp.*, vol. 17, no. 17, pp. 14627–14633, Aug. 2009.

[18] V. Singh *et al.*, "Mid-infrared materials and devices on a Si platform for optical sensing," *Sci. Technol. Adv. Mater.*, vol. 15, no. 1, Feb. 2014, Art. no. 014603.

[19] W. Bogaerts *et al.*, "Nanophotonic waveguides in silicon-on-insulator fabricated with CMOS technology," *J. Lightw. Technol.*, vol. 23, no. 1, pp. 401–412, Jan. 2005.

[20] D. X. Xu *et al.*, "Real-time cancellation of temperature induced resonance shifts in SOI wire waveguide ring resonator label-free biosensor arrays," *Opt. Exp.*, vol. 18, no. 22, pp. 22867–22879, Oct. 2010.

[21] O. C. Zienkiewicz, R. L. Taylor, and J. Z. Zhu, *The Finite Element Method: Its Basis and Fundamentals*. Oxford, U.K.: Butterworth-Heinemann, 2013.

[22] T. I. Zohdi, "An introduction to the finite-element method," in *Mechanical Engineers' Handbook: Materials and Mechanical Design*, vol. 1, 3rd ed., M. Kutz, Ed. Hoboken, NJ, USA: Wiley, 2005.

[23] C. Ciminelli *et al.*, "Label-free optical resonant sensors for biochemical applications," *Prog. Quantum Electron.*, vol. 37, no. 2, pp. 51–107, Mar. 2013.

[24] D. Lee, J. Bae, S. Hong, H. Yang, and Y. B. Kim, "Optimized antireflective silicon nanostructure arrays using nanosphere lithography," *Nanotechnology*, vol. 27, no. 21, May 2016, Art. no. 215302.

[25] A. Lacraz, M. Polis, A. Theodosiou, C. Koutsides, and K. Kalli, "Femtosecond laser inscribed bragg gratings in low loss CYTOP polymer optical fiber," *IEEE Photon. Technol. Lett.*, vol. 27, no. 7, pp. 693–696, Jan. 2015.
[26] C. Morenohernández *et al.*, "Optical fiber temperature sensor based on a microcavity with polymer overlay," *Opt. Exp.*, vol. 24, no. 5, pp. 5654–5661, Mar. 2016.
[27] R. S. Moshrefzadeh, M. D. Radcliffe, T. C. Lee, and S. K. Mohapatra, "Temperature dependence of index of refraction of polymeric waveguides," *J. Lightw. Technol.*, vol. 10, no. 4, pp. 420–425, Apr. 1992.
[28] F. Qiu, F. Yu, A. M. Spring, and S. Yokoyama, "Athermal silicon nitride ring resonator by photobleaching of disperse red 1-doped poly(methyl methacrylate) polymer," *Opt. Lett.*, vol. 37, no. 19, pp. 4086–4088, Oct. 2012.
[29] L. Liang *et al.*, "Low-power and high-speed thermo-optic switch using hybrid silica/polymer waveguide structure: design, fabrication and measurement," *J. Mod. Opt.*, vol. 59, no. 12, pp. 1084–1091, Jul. 2012.
[30] Y. Jr Hung, C. J. Wu, T. H. Chen, T. H. Yen, and Y. C. Liang, "Superior temperature-sensing performance in cladding-modulated si waveguide gratings," *J. Lightw. Technol.*, vol. 34, no. 18, pp. 4329–4335, Sep. 2016.
[31] H. T. Kim and M. Yu, "Cascaded ring resonator-based temperature sensor with simultaneously enhanced sensitivity and range," *Opt. Exp.*, vol. 24, no. 9, pp. 9501–9510, May 2016.
[32] C. H. Dong *et al.*, "Fabrication of high-Q polydimethylsiloxane optical microspheres for thermal sensing," *Appl. Phys. Lett.*, vol. 94, Jun. 2009, Art. no. 231119.
[33] J. M. Ward, Y. Yang, and S. N. Chormaic, "Highly sensitive temperature measurements with liquid-core microbubble resonators," *IEEE Photon. Technol. Lett.*, vol. 25, no. 23, pp. 2350–2353, Sep. 2013.
[34] C. Wang, Q. Quan, S. Kita, Y. Li, and M. Lončar, "Single-nanoparticle detection with slot-mode photonic crystal cavities," *Appl. Phys. Lett.*, vol. 106, no. 26, Jun. 2015, Art. no. 261105.
[35] L. Zhou, K. Okamoto, and S. J. B. Yoo, "Towards athermal slotted silicon microring resonators with UV-trimmable PMMA upper-cladding," in *Proc. Lasers Electro-Opt. Conf. Quantum Electron. Laser Sci. Conf.*, 2009, Paper CTuBB3.
[36] P. Liu and Y. Shi, "Simultaneous measurement of refractive index and temperature using a dual polarization ring," *Appl. Opt.*, vol. 55, pp. 3537–3541, May 2016.
[37] Y. Ma *et al.*, "Mach–Zehnder interferometer-based integrated terahertz temperature sensor," *IEEE J. Select. Topics Quantum Electron.*, vol. 23, no. 4, Jul. 2017, Art. no. 4601607.
[38] S. Y. Chou, P. R. Krauss, and P. J. Renstrom, "Imprint lithography with 25-nanometer resolution," *Science*, vol. 272, no. 5258, pp. 85–87, Apr. 1996.
[39] C. Chao and L. J. Guo, "Polymer microring resonators fabricated by nanoimprint technique," *J. Vacuum Sci. Technol. B*, vol. 20, no. 6, pp. 2862–2866, Nov./Dec. 2002.
[40] V. de Katrien, B. Irene, S. Etienne, B. Peter, and B. Roel, "Silicon-on-Insulator microring resonator for sensitive and label-free biosensing," *Opt. Exp.*, vol. 15, no. 12, pp. 7610–7615, Jun. 2007.
[41] X. Hu *et al.*, "Metamaterial absorber integrated microfluidic terahertz sensors," *Laser Photon. Rev.*, vol. 10, no. 6, pp. 962–969, Oct. 2016.
[42] B. R. Watts, Z. Zhang, C. Xu, X. Cao, and M. Lin, "Integration of optical components on-chip for scattering and fluorescence detection in an optofluidic devi ce," *Biomed. Opt. Exp.*, vol. 3, no. 11, pp. 2784–2793, Nov. 2012.
[43] A. Densmore *et al.*, "Silicon photonic wire biosensor array for multiplexed real-time and label-free molecular detection," *Opt. Lett.*, vol. 34, no. 23, pp. 3598–3600, Dec. 2009.
[44] G. Gervinskas, D. J. Day, and S. Juodkazis, "Optofluidic Fabry-Pérot sensor for water solutions at high flow rates," *Opt. Mater. Exp.*, vol. 2, no. 3, pp. 279–286, Mar. 2012.
[45] M. Soltani, J. Lin, S. Saraf, R. Forties, M. Lipson, and M. Wang, "Optofluidic electrical manipulation of individual biomolecules with nm-scale precision," in *Proc. CLEO, 2013 OSA Tech. Digest*, San Jose, CA, USA, 2013, Paper AM4M.3.